

# Jet Transport Coefficient at the Large Hadron Collider Energies in a Color String Percolation Approach

Aditya Nath Mishra<sup>1,\*</sup>, Dushmanta Sahu<sup>2,†</sup>, and Raghunath Sahoo<sup>2,3,‡</sup>

<sup>1</sup>*Wigner Research Centre for Physics, 29-33 Konkoly-Thege Miklós str., 1121 Budapest, Hungary*

<sup>2</sup>*Department of Physics, Indian Institute of Technology Indore, Simrol, Indore 453552, India and*

<sup>3</sup>*CERN, CH 1211, Geneva 23, Switzerland*

(Dated: May 29, 2022)

Within the color string percolation model (CSPM), jet transport coefficient,  $\hat{q}$ , is calculated for various multiplicity classes in proton-proton and for centrality classes in nucleus-nucleus collisions at the Large Hadron Collider energies for a better understanding of the matter formed in ultra-relativistic collisions.  $\hat{q}$  is studied as a function of final state charged particle multiplicity, initial state percolation temperature and energy density. The CSPM results are then compared with different theoretical calculations from the JET collaboration those incorporate particle energy loss in the medium. A good agreement is found between CSPM results and the JET collaboration calculations.

## I. INTRODUCTION

The main objective of tera-electron volt energy heavy-ion collisions is to form a Quark-Gluon Plasma (QGP)—the deconfined state of quarks and gluons, by creating extreme conditions of temperature and(or) energy density [1, 2], a scenario that might have been the case after few microseconds of the creation of the Universe. Jets, as collimated emission of multitude of hadrons originating from the hard partonic scatterings, play an important role as hard probes of QGP. These hard jets lose their energy through medium-induced gluon radiation and collisional energy loss, as a consequence of which one observes suppression of high transverse momentum particles and the phenomenon is known as jet quenching [3–9]. This is a direct signature of highly dense partonic medium, usually formed in high energy heavy-ion collisions. The first evidence of the jet quenching phenomenon has been observed at the Relativistic Heavy-Ion Collider (RHIC) [10–23] via the measurement of inclusive hadron and jet production at high  $p_T$ ,  $\gamma$ -hadron correlation, di-hadron angular correlations and the dijet energy imbalance. The jet quenching phenomena are also widely studied in heavy-ion collisions at the Large Hadron Collider (LHC) [24–38]. All the measured observables are found to be strongly modified in central heavy-ion collisions relative to minimum bias proton-proton collisions, when compared to expectations based on treating heavy-ion collisions as an incoherent superposition of independent nucleon-nucleon collisions.

A number of theoretical models that incorporate parton energy loss have been proposed to study the observed jet quenching phenomena, namely, Baier-Dokshitzer-Mueller-Peigne-Schiff-Zakharov (BDMPS-Z) [7, 39, 40], Gyulassy-Levai-Vitev (GLV) [41–43] and its CUJET im-

plementation [44], high-twist approach (HT-M and HT BW) [45–49], Amesto-Salgado-Wiedemann (ASW) [50, 51], Arnold-Moore-Yaffe (AMY) model [52, 53], MARTINI model [54], BAMPS model [55], and LBT model [56]. Most of the theoretical models assumed a static potential for jet-medium interactions which result in a factorized dependence of parton energy loss on the jet transport coefficient ( $\hat{q}$ ). The jet transport coefficient  $\hat{q}$ , which describes the average transverse momentum square transferred from the traversing parton, per unit mean free path is a widely used parameter that modulates the energy loss of jets in a strongly-interacting QCD medium [7, 9].  $\hat{q}$  is also related to the gluon distribution density of the medium and therefore characterizes the medium property as probed by an energetic jet [7, 57]. Thus the collision energy and system size dependence study of jet transport coefficient will not only improve our understanding of experimental results on jet quenching but also can directly provide some information about the internal structure of the hot and dense QCD matter [57, 58].

In the present work we study  $\hat{q}$  and its relation with various thermodynamic properties of the QCD matter, in the framework of the Color String Percolation Model (CSPM) [59–64] which is inspired by QCD. This can be used as an alternative approach to Color Glass Condensate (CGC). In CSPM, it is assumed that color strings are stretched between projectile and the target, which may decay into new strings via  $q\bar{q}$  pair production and subsequently hadronize to produce observed hadrons [65]. These color strings may be viewed as small discs in the transverse plane filled with color field created by colliding partons. The final state particles are produced by the Schwinger mechanism, emitting  $q\bar{q}$  pairs in this field [66]. With the increasing collision energy and size of the colliding nuclei, the number of strings grow and start interacting to form clusters in the transverse plane. This process is very much similar to discs in the 2-dimensional percolation theory [60, 62, 67, 68]. At a certain critical density, called critical percolation density ( $\xi_c \geq 1.2$ ), a macroscopic cluster appears that marks the percola-

\*e-mail: Aditya.Nath.Mishra@cern.ch

†e-mail: Dushmanta.Sahu@cern.ch

‡e-mail: Raghunath.Sahoo@cern.ch

tion phase transition [60, 62, 67–70]. The combination of the string density dependent cluster formation and the 2-dimensional percolation clustering phase transition, are the basic elements of the non-perturbative CSPM. In CSPM the Schwinger barrier penetration mechanism for particle production and the fluctuations in the associated string tension due to the strong string interactions make it possible to define a temperature. The critical density of percolation is related to the effective critical temperature and thus percolation may provide information on deconfinement in the high-energy collisions [63, 64]. The CSPM approach has been successfully used to describe the initial stages in the soft region in high-energy collisions [59, 64, 67, 71–76]. In addition to this, CSPM has also been very successful in estimating various thermodynamic and transport properties of the matter formed in ultra-relativistic energies [77–83].

The paper runs as follows: first, we present the formulation and methodology of CSPM approach in section II. In section III, we present the result obtained and related discussions. Finally, the important findings of this work are summarized in section IV.

## II. FORMULATION AND METHODOLOGY

In color string percolation model, the charged hadron multiplicity,  $\mu_n$ , reduces with increase of string interactions while the mean transverse momentum squared,  $\langle p_T^2 \rangle_n$ , of these charged hadrons increases, to conserve the total transverse momentum. The charged particle multiplicity  $\mu_n$  and the mean transverse momentum squared  $\langle p_T^2 \rangle_n$  of the particles produced by a cluster, are proportional to the color charge and color field, respectively [62, 64] and can be defined as

$$\mu_n = \sqrt{\frac{nS_n}{S_1}}\mu_1; \quad \langle p_T^2 \rangle_n = \sqrt{\frac{nS_1}{S_n}}\langle p_T^2 \rangle_1, \quad (1)$$

where  $\mu_1$  and  $\langle p_T^2 \rangle_1$  are the mean multiplicity and transverse momentum squared of particles produced from a single string with a transverse overlap area  $S_1 = \pi r_0^2$  with  $r_0 = 0.2$  fm [64], respectively. For the case when strings are just touching each other  $S_n = nS_1$ , and  $\mu_n = n\mu_1$ ,  $\langle p_T^2 \rangle_n = \langle p_T^2 \rangle_1$ . When strings fully overlap  $S_n = S_1$  and therefore  $\mu_n = \sqrt{n}\mu_1$  and  $\langle p_T^2 \rangle_n = \sqrt{n}\langle p_T^2 \rangle_1$ , so that the multiplicity is maximally suppressed and the  $\langle p_T^2 \rangle_n$  is maximally enhanced. This implies a simple relation between the multiplicity and transverse momentum  $\mu_n \langle p_T^2 \rangle_n = n\mu_1 \langle p_T^2 \rangle_1$ , which denotes the conservation of the total transverse momentum. In the thermodynamic limit, one can obtain the average value of  $nS_1/S_n$  for all the clusters [60, 62] as

$$\left\langle n \frac{S_1}{S_n} \right\rangle = \frac{\xi}{1 - e^{-\xi}} \equiv \frac{1}{F(\xi)^2}. \quad (2)$$

Here,  $F(\xi)$  is the color suppression factor by which the overlapping strings reduce the net-color charge of the strings. With  $F(\xi) \rightarrow 1$  as  $\xi \rightarrow 0$  and  $F(\xi) \rightarrow 0$  as  $\xi \rightarrow \infty$ , where  $\xi = \frac{N_s S_1}{S_n}$  is the percolation density parameter. Eq. (1) can be written as  $\mu_n = nF(\xi)\mu_0$  and  $\langle p_T^2 \rangle_n = \langle p_T^2 \rangle_1/F(\xi)$ . It is worth noting that CSPM is a saturation model similar to the Color Glass Condensate (CGC), where  $\langle p_T^2 \rangle_1/F(\xi)$  plays the same role as the saturation momentum scale  $Q_s^2$  in the CGC model [84, 85].

In the present work we have extracted  $F(\xi)$  in  $pp$  collisions at  $\sqrt{s} = 5.02$  and 13 TeV for various multiplicity classes using ALICE published results of transverse momentum spectra of charged particles [86]. In case of Pb-Pb collisions at  $\sqrt{s_{NN}} = 2.76$  and 5.02 TeV, [87] and Xe-Xe collisions at  $\sqrt{s_{NN}} = 5.44$  TeV [88],  $F(\xi)$  values have been obtained from the published centrality dependent transverse momentum spectra of charged particles by ALICE. To evaluate the initial value of  $F(\xi)$  from data, a parameterization of the experimental data of  $p_T$  distribution in low-energy  $pp$  collisions at  $\sqrt{s} = 200$  GeV (minimum bias), where strings have very low overlap probability, was used [67]. The  $p_T$  spectrum of charged particles can be described by a power-law [64]:

$$\frac{d^2 N_{ch}}{dp_T^2} = \frac{a}{(p_0 + p_T)^\alpha}, \quad (3)$$

where  $a$  is the normalisation factor and  $p_0$ ,  $\alpha$  are fitting parameters given as,  $p_0 = 1.98$  and  $\alpha = 12.87$  [64]. This parameterization is used in high multiplicity  $pp$  and centrality dependent heavy-ion (AA) collisions to take into account the interactions of the strings [64]. The parameter  $p_0$  in Eq. (3) is for independent strings and gets modified to

$$p_0 \rightarrow p_0 \left( \frac{\langle nS_1/S_n \rangle^{mod}}{\langle nS_1/S_n \rangle_{pp}} \right)^{1/4}. \quad (4)$$

Using Eq.(4) and Eq.(2) in Eq.(3), we get

$$\frac{d^2 N_{ch}}{dp_T^2} = \frac{a}{(p_0 \sqrt{F(\xi)_{pp}/F(\xi)^{mod}} + p_T)^\alpha}, \quad (5)$$

where  $F(\xi)^{mod}$  is the modified color suppression factor and is used in extracting  $F(\xi)$  both in  $pp$  and AA collisions. The spectra were fitted using Eq.(5) in the softer sector with  $p_T$  in the range 0.15 - 1.0 GeV/c. In  $pp$  collisions at low-energies only two strings are exchanged with low probability of interactions, so that  $\langle nS_1/S_n \rangle_{pp} \approx 1$ , which transforms Eq.(5) into

$$\frac{d^2 N_{ch}}{dp_T^2} = \frac{a}{(p_0 \sqrt{1/F(\xi)^{mod}} + p_T)^\alpha}. \quad (6)$$

In the thermodynamic limit, the color suppression factor  $F(\xi)$  is related to the percolation density parameter

$\xi$  as

$$F(\xi) = \sqrt{\frac{1 - e^{-\xi}}{\xi}}. \quad (7)$$

### III. RESULTS AND DISCUSSIONS

In the present work, we have extracted  $F(\xi)$  in the multiplicity dependent  $pp$  collisions at  $\sqrt{s} = 5.02$  and 13 TeV [86] and centrality dependent Pb-Pb collisions at  $\sqrt{s_{NN}} = 2.76$  and 5.02 TeV [87], and Xe-Xe collisions at  $\sqrt{s_{NN}} = 5.44$  TeV [88] from the charged particles  $p_T$  spectra measured in ALICE at the LHC.

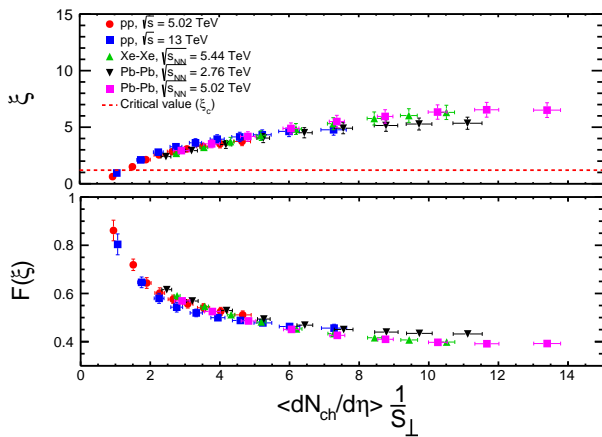


FIG. 1: (Color Online) Percolation density parameter,  $\xi$ , and color suppression factor,  $F(\xi)$ , as functions of charged particle multiplicity (within  $|\eta| < 0.8$ ) scaled with the transverse overlap area  $S_{\perp}$  in  $pp$ , Xe-Xe and Pb-Pb collisions are shown in upper and lower panel, respectively. For  $pp$  collisions multiplicity dependent  $S_{\perp}$  is obtained from IP-Glasma model [89]. In case of Xe-Xe and Pb-Pb collisions we use  $S_{\perp}$  values obtained using the Glauber model [90].

We show  $\xi$  and  $F(\xi)$  as functions of final charged particle multiplicity for  $pp$ , Xe-Xe and Pb-Pb collisions in Fig. 1 upper and lower panel, respectively. The error in  $F(\xi)$  is obtained by changing the fitting ranges of the transverse momentum spectra and is found within  $\sim 3\%$ . For a better comparison of proton-proton and nucleus-nucleus collisions,  $\langle dN_{ch}/d\eta \rangle$  is scaled by the transverse overlap area  $S_{\perp}$  for both  $pp$  and heavy-ion collisions. For  $pp$  collisions, multiplicity dependent  $S_{\perp}$  is calculated using the IP-Glasma model [89]. In the case of heavy-ion collisions the transverse overlap area was obtained using the Glauber model calculations [90]. It is observed that  $F(\xi)$  falls onto a universal scaling curve for proton-proton and nucleus-nucleus collisions. Particularly, in the most central heavy-ion collisions (high  $N_{tracks}$ ) and high multiplicity  $pp$  collisions,  $F(\xi)$  values fall in a line. This suggests that the color suppression factor is independent of collision energies and collision systems in the domain

of high final state multiplicity. Further, what decides the color suppression factor is the final state multiplicity density of the system, which turns out to be the initial parton density in a system for the case of an isentropic expansion.

#### A. Temperature

The connection between  $F(\xi)$  and the initial percolation temperature  $T(\xi)$  involves the Schwinger mechanism for particle production [63, 64, 66] and can be expressed as [63, 67]

$$T(\xi) = \sqrt{\frac{\langle p_T^2 \rangle_1}{2F(\xi)}}. \quad (8)$$

We adopt the point of view that the universal hadronization temperature is a good measure of the upper end of the cross-over phase transition temperature  $T_h$  [91]. The single string average transverse momentum  $\langle p_T^2 \rangle_1$  is calculated at the critical percolation density parameter  $\xi_c = 1.2$  with the universal hadronization temperature  $T_h = 167.7 \pm 2.6$  MeV [91]. This gives  $\sqrt{\langle p_T^2 \rangle_1} = 207.2 \pm 3.3$  MeV.

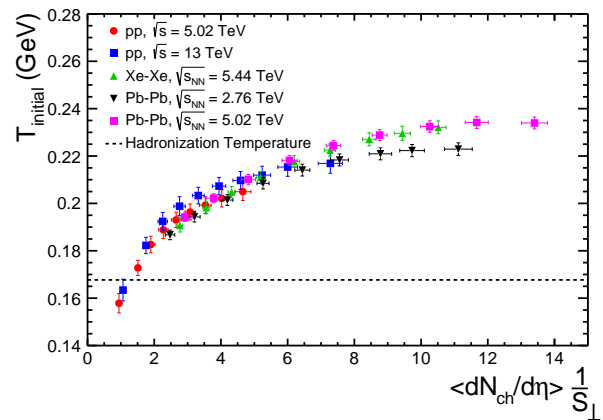


FIG. 2: (Color Online) Initial percolation temperature vs  $\langle dN_{ch}/d\eta \rangle$  scaled by  $S_{\perp}$  from  $pp$ , Pb-Pb and Xe-Xe collisions. The line  $\sim 167.7$  MeV is the universal hadronization temperature [91].

In this way at  $\xi_c = 1.2$  the connectivity percolation transition at  $T(\xi_c)$  models the thermal deconfinement transition. The temperature obtained for Au-Au collisions at  $\sqrt{s_{NN}} = 200$  GeV was  $\sim 193.6$  MeV which has reasonable agreement with the experimentally measured initial temperature  $T_i = 221 \pm 19^{stat} \pm 19^{sys}$  MeV by the PHENIX Collaboration [92]. The agreement with the measured temperature shows that the temperature obtained using Eq. (8) can be termed as the initial temperature of the percolation cluster.

Figure 2 shows a plot of initial temperature from CSPM as a function of  $\langle dN_{\text{ch}}/d\eta \rangle$  scaled by  $S_{\perp}$ . Temperatures from both  $pp$  and AA collisions fall on a universal curve when multiplicity is scaled by the transverse overlap area. The horizontal line at  $\sim 167.7$  MeV is the universal hadronization temperature obtained from the systematic comparison of the statistical thermal model parametrization of hadron abundances measured in high energy  $e^+e^-$ ,  $pp$  and AA collisions [91]. One can see that temperature for higher multiplicity classes in  $pp$  collisions at  $\sqrt{s} = 5.02$  and 13 TeV, are higher than the hadronization temperature and similar to those observed in Xe-Xe at  $\sqrt{s_{\text{NN}}} = 5.44$  TeV and Pb-Pb collisions at  $\sqrt{s_{\text{NN}}} = 2.76$  and 5.02 TeV.

### B. Energy density

The calculation of the bulk properties of hot QCD matter and characterization of the nature of the QCD phase transition is one of the most important and fundamental problems in finite-temperature QCD. The QGP according to CSPM is born in local thermal equilibrium because the temperature is determined at the string level. Beyond the initial temperature  $T > T_c$  the CSPM perfect fluid may expand according to Bjorken boost invariant 1-dimension hydrodynamics [93]. In this framework the energy density is given by:

$$\varepsilon = \frac{3}{2} \frac{dN_{\text{ch}}/dy \langle m_T \rangle}{S_{\text{N}} \tau_{\text{pro}}}, \quad (9)$$

where  $\varepsilon$  is the energy density,  $S_{\text{N}}$  is the transverse overlap area and  $\tau_{\text{pro}}$ , the production time for a boson (gluon), is described by [66]

$$\tau_{\text{pro}} = \frac{2.405\hbar}{\langle m_T \rangle}. \quad (10)$$

Here,  $m_T = \sqrt{m^2 + p_T^2}$  is the transverse mass. For evaluating  $\varepsilon$ , we use the charged particle multiplicity  $dN_{\text{ch}}/dy$  at mid-rapidity and  $m$  is taken as the pion mass (pions being the most abundant particles in a multiparticle production process like that is discussed here), which gives the lower bound of the energy density.

The purpose of estimating the initial percolation temperature and the initial energy density in the framework of CSPM is to study the jet transport coefficient as a function of these global observables for different collision species and collision energies at the LHC. Let us now proceed to estimate  $\hat{q}$  in the CSPM framework.

### C. Jet transport coefficient

The final state hadrons, produced in ultra-relativistic collisions at large transverse momenta are strongly suppressed in central collisions as compared to peripheral collisions. This suppression of hadrons at high  $p_T$ , which is usually referred to as jet quenching, is believed to be the result of the parton energy loss induced by multiple collisions in the strongly interacting medium. Thus, we are encouraged to study the jet transport coefficient,  $\hat{q}$ , which encodes the parton energy loss in the medium. It is also related to the  $p_T$  broadening of the energetic partons propagating inside the medium. In kinetic theory framework,  $\hat{q}$  can be estimated by the formula [94],

$$\hat{q} = \rho \int d^2q_{\perp} q_{\perp}^2 \frac{d\sigma}{d^2q_{\perp}}, \quad (11)$$

where  $\rho$  is the number density of the constituents of the medium and  $\frac{d\sigma}{d^2q_{\perp}}$  denotes the differential scattering cross-section of the particles inside the medium.

The transport parameter of jet quenching,  $\hat{q}$ , and the shear viscosity-to-entropy density ratio ( $\eta/s$ ), transport parameters describing the exchange of energy and momentum between fast partons and medium, are directly related to each other as [95–98]

$$\frac{\eta}{s} \approx \frac{3 T^3}{2 \hat{q}} \quad (12)$$

Within the CSPM approach, the shear viscosity-to-entropy density ratio,  $\eta/s$ , can be expressed as

$$\frac{\eta}{s} = \frac{TL}{5(1 - e^{-\xi})}, \quad (13)$$

here  $L$  is the longitudinal extension of the string  $\sim 1$  fermi [63]. One can get final expression for jet transport coefficient from Eq. 12 as:

$$\hat{q} \approx \frac{3 T^3}{2 \eta/s} \approx \frac{15 T^2 (1 - e^{-\xi})}{2 L} \quad (14)$$

The jet quenching parameter  $\hat{q}$  is plotted as a function of initial percolation temperature in Fig. 3. Interestingly, we observe a linear increase in  $\hat{q}$ , with the increase in temperature for both  $pp$  and AA collisions. At low temperatures, the value of jet quenching parameter is around  $0.02 \text{ GeV}^3$ . This value increases gradually and at high temperatures it reaches around  $0.08 \text{ GeV}^3$ .

The Jet collaboration has also extracted  $\hat{q}$  values from five different hydrodynamic approaches with the initial temperatures of  $T_0 = 346\text{-}373$  and  $447\text{-}486$  MeV for the most central Au-Au collisions at  $\sqrt{s} = 200$  GeV at RHIC and Pb-Pb collisions at  $\sqrt{s} = 2.76$  TeV at LHC, respectively. The variation of  $\hat{q}$  values between different hydrodynamic models are considered as theoretical uncer-

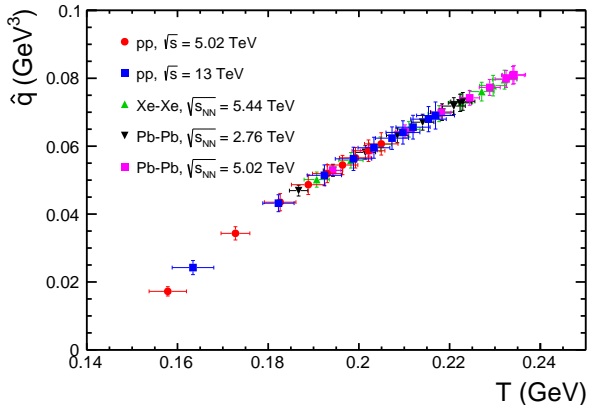


FIG. 3: (Color Online) Jet quenching parameter  $\hat{q}$  as a function of temperature within the CSPM for  $pp$  collisions at  $\sqrt{s} = 5.02$  and 13 TeV, Xe-Xe collisions at  $\sqrt{s_{NN}} = 5.44$  TeV and Pb-Pb collisions at  $\sqrt{s_{NN}} = 2.76$  and 5.02 TeV.

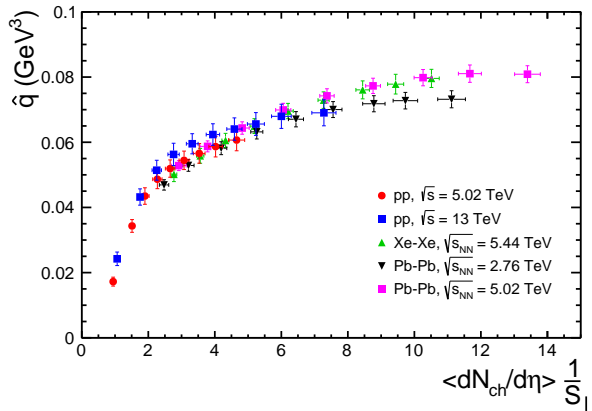


FIG. 4: (Color Online) Jet quenching parameter  $\hat{q}$  as a function charged particle multiplicity scaled with transverse overlap area ( $S_{\perp}$ ) within the CSPM for  $pp$  collisions at  $\sqrt{s} = 5.02$  and 13 TeV, Xe-Xe collisions at  $\sqrt{s_{NN}} = 5.44$  TeV and Pb-Pb collisions at  $\sqrt{s_{NN}} = 2.76$  and 5.02 TeV.

tainties. The scaled jet quenching parameter  $\hat{q}/T^3$  at the highest temperatures reached in the most central Au–Au and Pb–Pb collisions are [58]

$$\frac{\hat{q}}{T^3} \approx \begin{cases} 4.6 \pm 1.2 & \text{at RHIC} \\ 3.7 \pm 1.4 & \text{at LHC.} \end{cases}$$

The corresponding absolute values for  $\hat{q}$  for a 10 GeV quark jet are,

$$\hat{q} \approx \begin{cases} 0.23 \pm 0.05 \\ 0.37 \pm 0.13 \end{cases} \text{ GeV}^3 \text{ at } \begin{cases} T = 346\text{-}373 \text{ MeV (RHIC),} \\ T = 447\text{-}486 \text{ MeV (LHC),} \end{cases}$$

at an initial time  $\tau_0 = 0.6$  fm/c. In this work, we

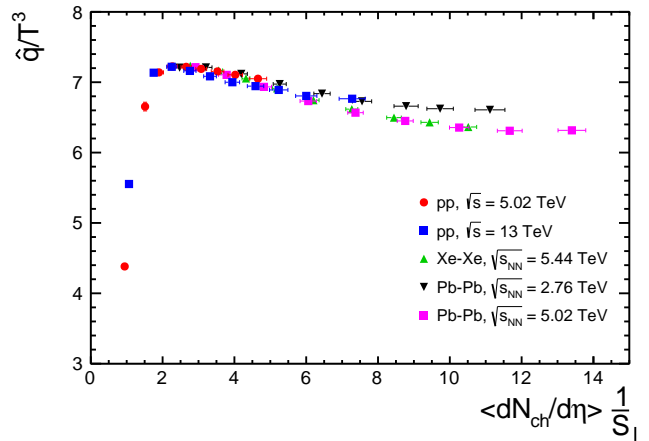


FIG. 5: (Color Online)  $\hat{q}/T^3$  vs charged particle multiplicity scaled by  $S_{\perp}$  for  $pp$  collisions at  $\sqrt{s} = 5.02$  and 13 TeV, Xe-Xe collisions at  $\sqrt{s_{NN}} = 5.44$  TeV and Pb-Pb collisions at  $\sqrt{s_{NN}} = 2.76$  and 5.02 TeV.

use charged particle spectra to calculate  $\hat{q}$  within CSPM approach, so we can't reach at the initial temperature published by the JET collaboration. Therefore, our  $\hat{q}$  is significantly smaller than the value published by the JET collaboration for the most central Pb-Pb collisions at  $\sqrt{s} = 2.76$  TeV at the LHC.

In Fig. 4, we have plotted  $\hat{q}$  as a function of charged particle multiplicity scaled with transverse overlap area for  $pp$  collisions at  $\sqrt{s} = 5.02$  and 13 TeV, Xe-Xe collisions at  $\sqrt{s_{NN}} = 5.44$  TeV and Pb-Pb collisions at  $\sqrt{s_{NN}} = 2.76$  and 5.02 TeV. One can see that  $\hat{q}$  shows a steep increase at lower charged particle multiplicities in  $pp$  collisions and gets saturated at very high multiplicity for all studied energies. This behaviour suggests that at lower multiplicities, the system is not dense enough to highly quench the partonic jets, whereas with increase of multiplicity the quenching of jets becomes more prominent.

The dimensionless parameter,  $T^3$ -scaled  $\hat{q}$  is shown in Fig. 5 as a function of charged particle multiplicity scaled with transverse overlap area. In the low multiplicity regime we observe a steep increase in  $\hat{q}/T^3$ , and after reaching to a maximum at  $\langle dN_{ch}/d\eta \rangle / S_{\perp} \sim 2$  it starts decreasing regardless of the collision system or collision energy. The decrease in  $\hat{q}/T^3$  is faster in Pb-Pb and Xe-Xe as compared to the  $pp$  collisions.

The variation of  $\hat{q}$  as a function of initial energy density is shown in Fig. 6. To have a better understanding, we have compared our results with that of cold nuclear matter, massless hot pion gas and ideal QGP calculations [99]. We observe that at low energy density, our result within CSPM is very close to the massless hot pion gas which suggests that the systems behave almost like massless hot pion gas. As initial energy density increases, our results deviate from that of the ideal QGP. This is understandable due to the fact that the system formed in high multiplicity events are actually viscous and are not exactly ideal. The saturation behaviour observed at high

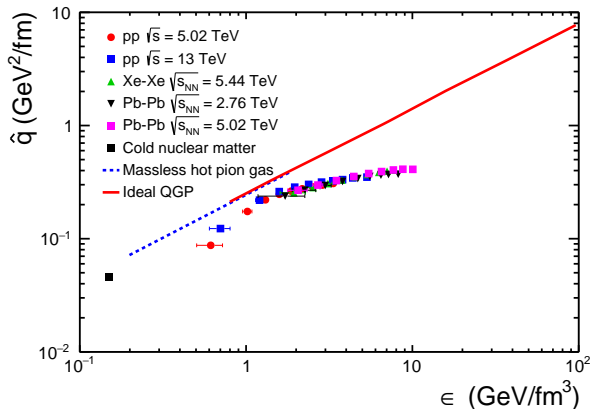


FIG. 6: (Color Online) Jet quenching parameter  $\hat{q}$  as a function of initial energy density for  $pp$  collisions at  $\sqrt{s} = 5.02$  and 13 TeV, Xe-Xe collisions at  $\sqrt{s_{NN}} = 5.44$  TeV and Pb-Pb collisions at  $\sqrt{s_{NN}} = 2.76$  and 5.02 TeV. The blue dotted line is for massless pion gas, the solid red curve is for ideal QGP and the black square is for cold nuclear matter [99].

energy density suggest that after a certain energy density  $\hat{q}$  remain unaffected. The similar behaviour is observed when  $\hat{q}$  is studied as a function of multiplicity (shown in Fig. 4).

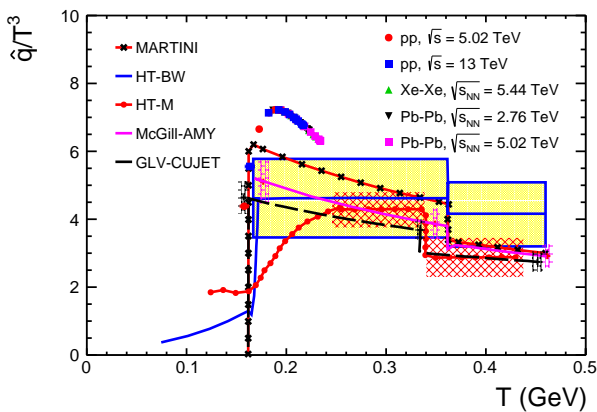


FIG. 7: (Color Online) Scaled jet quenching parameter  $\hat{q}/T^3$  as a function of initial temperature for  $pp$  collisions at  $\sqrt{s} = 5.02$  and 13 TeV, Xe-Xe collisions at  $\sqrt{s_{NN}} = 5.44$  TeV and Pb-Pb collisions at  $\sqrt{s_{NN}} = 2.76$  and 5.02 TeV.

In Fig. 7, we have plotted  $\hat{q}/T^3$  as a function of initial temperature. For the comparison, we have also plotted the results obtained by the JET collaboration using five different theoretical models that incorporate particle energy loss in the medium. The GLV model [41–43] predicted the general form of the evolution of center-of-mass energy of the high transverse momentum pion nuclear modification factor from Super Proton Synchrotron (SPS) and RHIC to LHC energies. CUJET 1.0 explained

the similarity between  $R_{AA}$  at RHIC and LHC, despite the fact that the initial QGP density in LHC almost doubles that of RHIC, by taking the effects due to multi-scale running of the QCD coupling  $\alpha(Q^2)$  into account [44]. In CUJET 2.0, the CUJET 1.0 is coupled with the 2+1D viscous hydro fields. By taking GLV-CUJET, the JET collaboration has estimated the scaled  $\hat{q}$ , which is shown by the dashed black line. The Higher-Twist Berkeley-Wuhan (HT-BW) model uses a 3+1D ideal hydrodynamics to provide the space-time evolution of the local temperature and the flow velocity in the medium along the jet propagation path in heavy-ion collisions. The result obtained from HT-BW model is represented by the blue line. The Higher-Twist Majumder (HT-M) model (red line with filled circles) uses a 2+1D viscous hydrodynamic model to provide the space-time evolution of the entropy density [45–49]. The nuclear initial parton scatterings for jet production are carried out by using PYTHIA8 in the MARTINI model [54]. This model describes the suppression of hadron spectra in heavy-ion collisions at RHIC very well with a fixed value of strong coupling constant. The MARTINI model calculation is represented by red line with black crosses. In MCGILL-AMY model [52, 53], the scattering and radiation processes are described by thermal QCD and hard thermal loop (HTL) effects [100] and Landau-Pomeranchuk-Migdal (LPM) interference [101]. In this approach, a set of rate equations for their momentum distributions are solved to obtain the evolution of hard jets (quarks and gluons) in the hot QCD medium. The result obtained from this model is represented by the magenta line. We observe that  $\hat{q}/T^3$  obtained from CSPM approach has similar kind of behaviour as observed by JET collaboration.

#### IV. CONCLUSION

We study the thermodynamic and transport properties of the matter formed in  $pp$  and AA collisions at LHC energies within the framework of the CSPM. We extract percolation density parameter by fitting transverse momentum spectra within Color String Percolation Model and then calculate initial percolation temperature ( $T$ ), energy density ( $\epsilon$ ) and the jet transport coefficient ( $\hat{q}$ ). In the present work, for the first time we study the jet transport coefficient of produced hot QCD matter within the color string percolation approach at the LHC energies. We show that  $\hat{q}$  increases linearly with initial temperature regardless of the collision system or collision energy.

At very low multiplicity,  $\hat{q}$  shows a sharp increase and this dependence becomes weak at high multiplicity (energy density). This behaviour suggests that at lower multiplicity, the system is not dense enough to highly quench the partonic jets, whereas with increase of multiplicity the quenching of jets becomes more prominent. At very high multiplicity (energy density)  $\hat{q}$  saturates with multiplicity (energy density) which allows us to make a conclu-

sion that at very high multiplicity (high energy density)  $\hat{q}$  becomes independent of final state multiplicity when scaled by transverse overlap area of the produced fireball. Interestingly, we found that  $\hat{q}$  in the low energy density regime, the system behaves almost like a massless hot pion gas. As initial energy density increases,  $\hat{q}$  values deviate from the ideal QGP values because of the fact that systems produced in high multiplicity events are actually viscous and are not exactly ideal. The  $\hat{q}/T^3$  obtained from CSPM approach as a function of temperature has similar kind of behaviour as observed by the JET collaboration using five different theoretical models that incorporate particle energy loss in the medium.

In view of heavy-ion-like signatures seen in TeV high-multiplicity  $pp$  collisions at the LHC energies, it would be really exciting to see the jet quenching results in such collisions to infer about the possible QGP-droplet formation. The present study of jet transport coefficient as

a function of final state multiplicity, initial temperature and energy density will pave a way for such an experimental exploration making LHC  $pp$  collisions unique.

### Acknowledgements

A. N. M. would like to thank the Hungarian National Research, Development and Innovation Office (NKFIH) under the contract numbers OTKA K135515, K123815 and NKFIH 2019-2.1.11-T ET-2019-00078, 2019-2.1.11-T ET-2019-00050 and the Wigner GPU Laboratory. R.S. acknowledges the financial supports under the CERN Scientific Associateship and the financial grants under DAE-BRNS Project No. 58/14/29/2019-BRNS of the Government of India.

- 
- [1] J. D. Bjorken, Technical Report FERMILAB-PUB-82-059-T, 1982.
  - [2] D. d'Énterria, "Jet quenching", in Relativistic Heavy Ion Physics, R. Stock, ed., volume 23, p. 99, 2010, arXiv:0902.2011.
  - [3] J. P. Blaizot and L. D. McLerran, Phys. Rev. D **34**, 2739 (1986).
  - [4] M. Gyulassy and M. Plumer, Phys. Lett. B **243**, 432 (1990).
  - [5] X. N. Wang and M. Gyulassy, Phys. Rev. Lett. **68**, 1480 (1992)
  - [6] R. Baier, Y. L. Dokshitzer, S. Peigne and D. Schiff, Phys. Lett. B **345**, 277 (1995).
  - [7] R. Baier, Y. L. Dokshitzer, A. H. Mueller, S. Peigne, and D. Schiff, Nucl. Phys. B **484**, 1265 (1997).
  - [8] G. Y. Qin and X. N. Wang, Int. J. Mod. Phys. E **24**, 1530014 (2015).
  - [9] M. Gyulassy, I. Vitev, X.-N. Wang, and B.-W. Zhang, "Jet quenching and radiative energy loss in dense nuclear matter," in Quark-Gluon Plasma, R. C. Hwa and X.-N. Wang, Eds., p. 123, World Scientific, Singapore, 2004.
  - [10] K. Adcox *et al.* (PHENIX Collaboration), Phys.Rev. Lett. **88**, 022301 (2002).
  - [11] C. Adler *et al.* (STAR Collaboration) Phys. Rev. Lett. **90**, 082302 (2003).
  - [12] K. Adcox *et al.* (PHENIX Collaboration) Phys. Lett. **B561**, 82 (2003).
  - [13] S. S. Adler *et al.* (PHENIX Collaboration) Phys. Rev. Lett. **91**, 072301 (2003).
  - [14] J. Adams *et al.* (STAR Collaboration) Phys. Rev. Lett. **91**, 172302 (2003).
  - [15] J. Adams *et al.* (STAR Collaboration) Phys. Rev. Lett. **91**, 072304 (2003).
  - [16] B. Back *et al.* (PHOBOS Collaboration) Phys. Lett. B **578**, 297 (2004).
  - [17] I. Arsene *et al.* (BRAHMS Collaboration) Phys. Rev. Lett. **91**, 072305 (2003).
  - [18] A. Adare *et al.* (PHENIX Collaboration) Phys. Rev. Lett. **98**, 232302 (2007).
  - [19] S. S. Adler *et al.* (PHENIX Collaboration) Nucl. Phys. A **757**, 184 (2005).
  - [20] J. Adams *et al.* (STAR Collaboration) Nucl. Phys. A **757**, 102 (2005).
  - [21] B. Back *et al.* (PHOBOS Collaboration) Nucl. Phys. A **757**, 28 (2005).
  - [22] I. Arsene *et al.* (BRAHMS Collaboration) Nucl. Phys. A **757**, 1 (2005).
  - [23] A. Adare *et al.* (BRAHMS Collaboration) Phys. Rev. C **77**, 064907 (2008).
  - [24] K. Aamodt *et al.* (ALICE Collaboration) Phys. Lett. **B 696**, 30 (2011).
  - [25] G. Aad *et al.* (ATLAS Collaboration) Phys. Rev. Lett. **105**, 252303 (2010).
  - [26] S. Chatrchyan *et al.* (CMS Collaboration) Phys. Rev. C **84**, 024906 (2011).
  - [27] S. Chatrchyan *et al.* (CMS Collaboration) JHEP **1108**, 141 (2011).
  - [28] K. Aamodt *et al.* (ALICE Collaboration) Phys. Rev. Lett. **108**, 092301 (2012).
  - [29] S. Chatrchyan *et al.* (CMS Collaboration) Eur. Phys. J. **C 72**, 1945 (2012).
  - [30] S. Chatrchyan *et al.* (CMS Collaboration) Phys. Lett. **B 712**, 176 (2012).
  - [31] S. Chatrchyan *et al.* (CMS Collaboration) JHEP **1210**, 087 (2012).
  - [32] S. Chatrchyan *et al.* (CMS Collaboration) Phys. Lett. **B 718**, 773 (2013).
  - [33] G. Aad *et al.* (ATLAS Collaboration) Phys. Lett. **B 719**, 220 (2013).
  - [34] S. Chatrchyan *et al.* (CMS Collaboration) Phys. Rev. Lett. **113**, 132301 (2014).
  - [35] S. Chatrchyan *et al.* (CMS Collaboration) Phys. Lett. **B 730**, 243 (2014).
  - [36] S. Chatrchyan *et al.* (CMS Collaboration) Phys. Rev. **C 90**, 024908 (2014).
  - [37] G. Aad *et al.* (ATLAS Collaboration) Phys. Lett. **B 739**, 320 (2014).
  - [38] G. Aad *et al.* (ATLAS Collaboration) Phys. Rev. Lett. **114**, 072302 (2015).

- [39] B. Zakharov, JETP Lett. **63**, 952 (1996).
- [40] R. Baier, Y. L. Dokshitzer, A.H. Mueller, S. Peigne and D. Schiff, Nucl. Phys. B **483**, 291 (1997).
- [41] M. Gyulassy, P. Levai and I. Vitev, Nucl. Phys. B **571**, 197 (2000).
- [42] M. Gyulassy, P. Levai and I. Vitev, Phys. Rev. Lett. **85**, 5535 (2000).
- [43] M. Gyulassy, P. Levai and I. Vitev, Nucl. Phys. B **594**, 371 (2001).
- [44] A. Buzzatti and M. Gyulassy, Phys. Rev. Lett. **108**, 022301 (2012).
- [45] X. F. Guo and X. N. Wang, Phys. Rev. Lett. **85**, 3591 (2000).
- [46] X.-N. Wang and X.-F. Guo, Nucl. Phys. A **696**, 788 (2001).
- [47] X. F. Chen, T. Hirano, E. Wang, X. N. Wang and H. Zhang, Phys. Rev. C **84**, 034902 (2011).
- [48] A. Majumder, Phys. Rev. D **85**, 014023 (2012).
- [49] I. Vitev and B. W. Zhang, Phys. Rev. Lett. **104**, 132001 (2010)
- [50] U. A. Wiedemann, Nucl. Phys. B **588**, 303 (2000).
- [51] U. A. Wiedemann, Nucl. Phys. A **690**, 731 (2001).
- [52] P.B. Arnold, G.D. Moore and L.G. Yaffe, JHEP **0111**, 57 (2001).
- [53] P.B. Arnold, G.D. Moore and L.G. Yaffe, JHEP **0206**, 30 (2002).
- [54] B. Schenke, C. Gale and S. Jeon, Phys. Rev. C **80**, 054913 (2009).
- [55] O. Fochler, Z. Xu and C. Greiner, Phys. Rev. C **82**, 024907 (2010).
- [56] Y. He, T. Luo, X. N. Wang and Y. Zhu, Phys. Rev. C **91**, 054908 (2015), Erratum: [Phys. Rev. C **97**, no. 1, 019902 (2018)].
- [57] J. Casalderrey-Solana and X. N. Wang, Phys. Rev. C **77**, 024902 (2008).
- [58] K. M. Burke *et al.* (JET Collaboration), Phys. Rev. C **90**, 014909 (2014).
- [59] N. Armesto *et al.*, Phys. Rev. Lett. **77**, 3736 (1996).
- [60] M. A. Braun and C. Pajares, Eur. Phys. J. C **16**, 349 (2000).
- [61] M. A. Braun and C. Pajares, Phys. Rev. Lett. **85**, 4864 (2000).
- [62] M. A. Braun, F. del Moral and C. Pajares, Phys. Rev. C **65**, 024907 (2002).
- [63] J. Dias de Deus, C. Pajares, Phys. Lett. B **642**, 455 (2006).
- [64] M. A. Braun *et al.*, Phys. Rep. **599**, 1 (2015).
- [65] M. A. Braun, F. del Moral, and C. Pajares, Nucl. Phys. A **715**, 791 (2003).
- [66] J. Schwinger, Phys. Rev. **128**, 2425 (1962).
- [67] R. P. Scharenberg, B. K. Srivastava and A. S. Hirsch, Eur. Phys. J. C **71**, 1510 (2011).
- [68] M. B. Isichenko, Rev. Mod. Phys. **64**, 961 (1992).
- [69] H. Satz, Rep. Prog. Phys. **63**, 1511 (2000).
- [70] A. N. Mishra *et al.*, *PoS LHCP2019* (2019) 004.
- [71] L. Cunqueiro, J. Dias de Deus, C. Pajares, Eur. Phys. J. C **65**, 423 (2010).
- [72] C. Andres, A. Moscoso and C. Pajares, Phys. Rev. C **90**, 054902 (2014).
- [73] R. P. Scharenberg, *PoS CPOD 2013*, 017 (2013).
- [74] J. Dias de Deus *et al.*, Eur. Phys. J. C **72**, 2123 (2012).
- [75] B. K. Srivastava, Nucl. Phys. A **926**, 142 (2014).
- [76] J. Dias de Deus *et al.*, Phys. Rev. C **93**, 024915 (2016).
- [77] P. Sahoo, S. De, S. K. Tiwari and R. Sahoo, Eur. Phys. J. A **54**, 136 (2018).
- [78] P. Sahoo, S. K. Tiwari, S. De, R. Sahoo, R. P. Scharenberg and B. K. Srivastava, Mod. Phys. Lett. A **34**, 1950034 (2019).
- [79] P. Sahoo, R. Sahoo and S. K. Tiwari, Phys. Rev. D **100**, 051503 (2019).
- [80] P. Sahoo, S. K. Tiwari and R. Sahoo, Phys. Rev. D **98**, 054005 (2018).
- [81] D. Sahu, S. Tripathy, R. Sahoo and S. K. Tiwari, arXiv:2001.01252 [hep-ph].
- [82] D. Sahu and R. Sahoo, arXiv:2006.04185 [hep-ph].
- [83] A. N. Mishra, G. Paic, C. Pajares, R. P. Scharenberg and B. K. Srivastava, arXiv:2006.10169 [hep-ph].
- [84] L. McLerran and R. Venugopalan, Phys. Rev. D **49**, 2233 (1994).
- [85] J. Dias de Deus and C. Pajares, Phys. Lett. B **695**, 211 (2011).
- [86] S. Acharya *et al.* (ALICE Collaboration), Eur. Phys. J. C **79**, 857 (2019).
- [87] J. Acharya *et al.* (ALICE Collaboration), JHEP **11**, 013 (2018).
- [88] J. Adam *et al.* (ALICE Collaboration), Phys. Lett. B **788**, 166 (2019).
- [89] L. McLerran, M. Praszalowicz, and B. Schenke, Nucl. Phys. A **916**, 210 (2013).
- [90] C. Loizides, Phys. Rev. C **94**, 024914 (2016).
- [91] F. Becattini, P. Castorina, A. Milov and H. Satz, Eur. Phys. J. C **66**, 377 (2010).
- [92] K. Adcox *et al.* (PHENIX Collaboration), Nucl. Phys. A **757**, 184 (2005).
- [93] J. D. Bjorken, Phys. Rev. D **27** 140 (1983).
- [94] R. Baier and Y. Mehtar-Tani, Phys. Rev. C **78**, 064906 (2008).
- [95] H. Liu, K. Rajagopal and U. A. Wiedemann, Phys. Rev. Lett. **97**, 182301 (2006).
- [96] A. Majumder, B. Muller and X. N. Wang, Phys. Rev. Lett. **99**, 192301 (2007).
- [97] Jorge Casalderrey-Solana and Xin-Nian Wang, Phys. Rev. C **77**, 024902 (2008)
- [98] J. Xu, Nucl. Sci. Tech. **24**, 50514 (2013).
- [99] R. Baier, Nucl. Phys. A **715**, 209 (2003).
- [100] N. Su, Commun. Theor. Phys. **57**, 409 (2012).
- [101] R. Baier, Y. L. Dokshitzer, A. H. Mueller, S. Peigne, S. Peigne and D. Schiff, Nucl. Phys. B **478**, 577 (1996).